Physics Status of NICA/MPD Project at JINR

V. D. Kekelidze, R. Lednicky, G. Musulmanbekov*, A. S. Sorin
For the NICA/MPD Collaboration
Joint Institute for Nuclear Research
Dubna

Abstract

The scientific program of the new NICA/MPD project, proposed for a study of a hot and dense hadronic matter created in heavy ion collisions over the atomic mass range A = 1–197 at a centre-of-mass energy up to $\sqrt{s_{NN}} = 11\ GeV$, is presented. The observables which are presumably sensitive to high density effects and phase transitions are discussed.

1 Introduction

The new Nuclotron-based Ion Collider fAcility (NICA) with the MultiPurpose Detector (MPD) being a flagship project at JINR is planned to study hot and dense baryonic matter in the energy region of $\sqrt{s_{NN}} = 4$ - 11 GeV by means of careful scanning in beam energy, atomic number and centrality of the excitation functions. Investigation of hot and dense baryonic matter provides information on the in-medium properties of hadrons and nuclear matter equation of state, allows a search for possible manifestations of the deconfinement and/or chiral symmetry restoration, phase transition, mixed phase and critical end point, and sheds light on the evolution of the Early Universe and formation of neutron stars.

The global scientific goal of the NICA/MPD Project is to explore the phase diagram of strongly interacting matter in the region of highly compressed and hot baryonic matter. Such matter exists in neutron stars and in the core of supernova explosions, while in the early Universe we meet the opposite conditions of very high temperature and vanishing baryonic density. In terrestrial experiments, high-density nuclear matter can transiently be created in a finite reaction volume in relativistic heavy ion collisions. In these collisions, a large fraction of the beam energy is converted into newly created hadrons, and new color degrees of freedom [9, 34] may be excited. The properties of excited resonances may noticeably be modified by the surrounding hot and dense medium. At very high temperature or density, this hadron mixture melts and their constituents, quarks and gluons, form a new phase of matter, the quark-gluon plasma. Different phases of strongly interacting matter are shown in the phase diagram on Figure 1. As it is seen from the phase diagram, the heavy-ion experiments at BNL-RHIC and CERN-LHC probe the region of high temperature and low net baryon density where circumstantial evidence has been obtained for a new phase, strongly interacting quak-gluon matter existing above a critical temperature $T_{cp} \approx 160 - 170$ MeV. In the other corner of the phase diagram, at lower temperature and moderate baryonic density, the GSI-SIS experiments definitely show no hint at a phase transition but certainly point to in-medium modification effects. At still higher density and low temperature there are theoretical predictions that the matter is deconfined and, correlated quark-antiquark pairs form a color superconductive phase. Such phase may be created in the interior of neutron stars. We are interested in an intermediate region of the phase diagram, where essential evidence was obtained by the NA49 collaboration

*e-mail: genis@jinr.ru

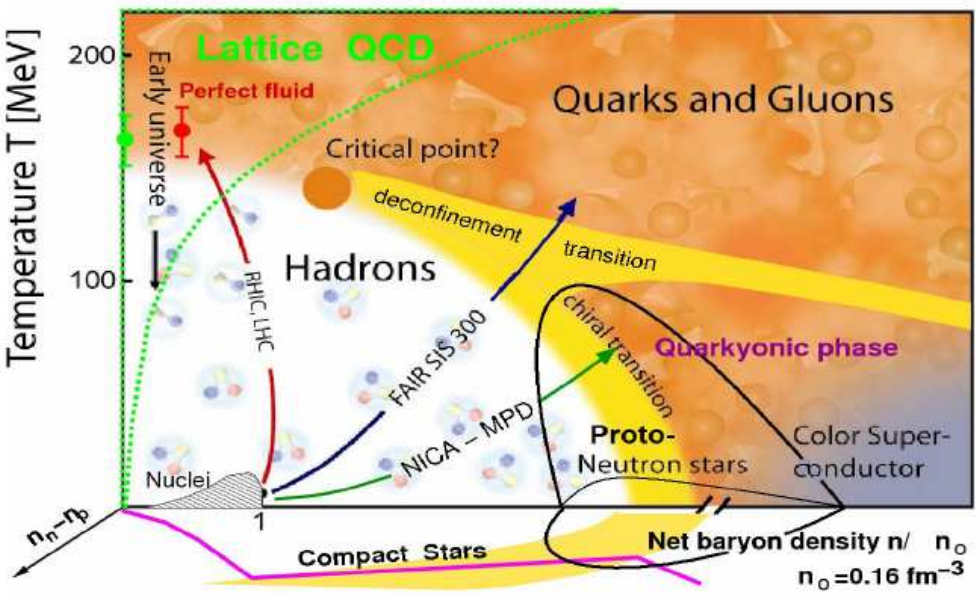

Figure 1: The phase diagram of strongly interacting QCD matter with the NICA domain added. Phase boundaries, critical end-point, and conjectured dynamical trajectories for an expansion stage are plotted as well.

within the CERN-SPS energy scan program that the system enters a new phase at a beam energy of about 30 AGeV. The fascinating particularity of this energy range is the critical end point possibly located according to the recent lattice QCD calculations at $T_{cp} = (162\pm 2)$ MeV and baryon chemical potential $\mu_{cp} = (360\pm 40)$ MeV [12], whereas model predictions are strongly scattered throughout the regions of $T_{cp} \sim 50-170$ Mev and $\mu_{cp} \sim 200-1400$ MeV [33] The importance of this finding was well understood at GSI where the CBM (Compressed Baryon Matter) experiment was proposed within the FAIR project. This understanding was recently shared by the BNL-RHIC which suggested to decrease its beam collider energy up to $\sqrt{s}_{NN} =$ 5 GeV to reach this domain of the phase diagram. The beam energy of the NICA is very much lower than those of the RHIC and the LHC, but it sits right on top of the region where the baryon density at the freeze-out is expected to be the highest. In this energy range, the excited system occupies a maximal space-time volume in the mixed quark-hadron phase the coexistence phase of hadron and quark-qluon matter. Therefore, the major goals of the NICA/MPD Project are investigations of in-medium properties of hadrons and the nuclear matter equation of state, including a search for possible signals of deconfinement and/or chiral symmetry restoration phase transitions and the QCD critical endpoint. Due to the high complexity of this task and large uncertainty in the predicted signals, an accurate scanning of the considered phase diagram domain in collision energy, impact parameter, and system size is utterly needed.

2 MPD - MultiPurpose Detector

The design concept of a detector which would be capable to exploit the broad physics potential of the high luminosity NICA collider is a challenging task. The detector to explore phase diagram of strongly interacting matter in a high track multiplicity environment has to cover a large phase space, be functional at high interaction rates and comprise high efficiency and excellent particle identification capabilities. It must also be based on the recent detector developments in order to meet the ambitious physics requirements, and to be of comparatively reasonable cost. None of the existing and planned so far experimental facilities can fulfill all these demands. The MPD

detector will be operated at an interaction rate of about $7 \cdot 10^3$ interactions per second with multiplicities of up to ~1500 charged particles per central $Au + Au$ collision at the maximal energy. This interaction rate provides more than two orders of magnitude advantage over the low-energy RHIC. The intensity of the planned fixed target CBM experiment is higher by almost three orders of magnitude, however it will have non-homogeneous acceptance depending on the beam energy, while the MPD acceptance is homogeneous in the whole energy range. The MPD detector design is shown in Fig. 2. It comprises the central detector (CD) and two forward spectrometers FS-A and FS-B (optional) situated along the beam line symmetrically with respect to the center of MPD. The detector design parameters follow from several technical constrains and guided by good detector performances versus a reasonable budget compromise. The CD consists of a barrel part and two end-caps (ECT) located inside the magnetic field.

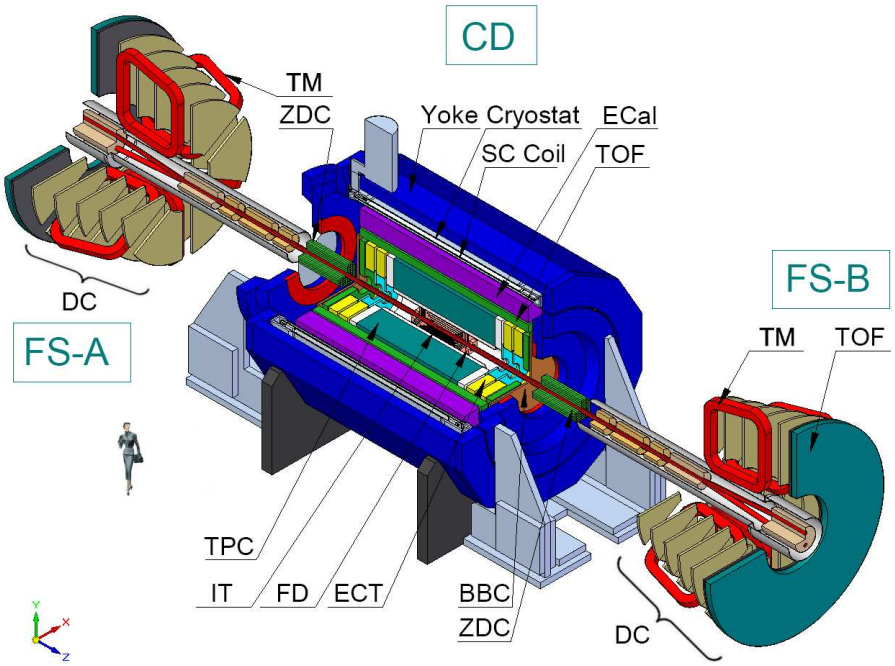

Figure 2: General view of the MPD detector with end doors retracted for access to the inner detector components. The detector is represented by three major parts: CD-central parts, and (FS-A, FS-B) - two forward spectrometers (optional). The subsystems are indicated: superconductor solenoid (SC Coil) and magnet yoke, inner detector (IT), end-cup tracker (ECT), time-projection chamber (TPC), time-of-flight stop counters (TOF), electromagnetic calorimeter (EMC), fast forward detectors (FFD), beam-beam counter (BBC), and zero degree calorimeter (ZDC).

The barrel part is a shell-like set of various detector systems surrounding the interaction point and aimed to reconstruct and identify both charged and neutral particles in the pseudorapidity region of $|\eta| \leq 1.2$. The endcaps are aimed for precise tracking over pseudorapidity range ($1.2 < |\eta| < 2$). Two forward magnet spectrometers (FS-A and FS-B) considered as optional are situated on both sides of MPD barrel and cover the pseudorapidity region from 2.0 to 3.0.

3 The Observables

In order to reach the goals of the project, the envisaged experimental programme includes the simultaneous measurement of the observables which are presumably sensitive to high density ef-

fects and phase transitions. The obsevables measured on event-by-event basis are particle yields and ratios, correlations and fluctuations. If the QCD critical point, CP, exists, substantial critical phenomena such as large non-statistical fluctuations and correlations in the particle yield and kinematical spectra are expected. Different species probe different stages of the nucleus-nucleus interaction due to their differences in mass, energy and interaction cross sections. The hadrons containing strange quarks are of particular interest because they are created in the early (high-temperature/high-density) stage of nucleus-nucleus collision and subsequently possess low interaction cross sections with surrounding matter. Among various characteristics, the elliptic flow deserves special attention because this collective motion is formed mainly in the early stage of the collision. The spatio-temporal information on the particle freeze-out source, which depends on the preceding evolution of the system, is provided by the measurement of fermtoscopic particle correlations. Certainly, the direct information on hot and dense transient matter is provided by penetrating probes, photons and leptons. In this respect, the vector mesons which contain information on chiral symmetry restoration are very attractive. Several unexpected results at lower energies were obtained in the NA49 experiment at SPS: non-monotonic K^+/π^+ behavior, "horn-effect" and hardening of kaon transverse momentum spectra at $\sqrt{s}_{NN} \approx 7$ GeV, and the "collapse"of proton direct flow. The energy scan which will be undertaken by RHIC, FAIR, NICA, SPS aim to study the evolution with beam energy of the unusual medium properties found at RHIC: do any of the partonic properties change or "turn off"? The following observables are planned for studying by all these collaborations during the energy scan:

- Multiplicity and spectral characteristics of the identified hadrons including strange particles, multi-strange baryons characterizing entropy production and system temperature at freeze-out.
- Event-by-event fluctuations in multiplicity, charges, transverse momenta and K/π ratios as a generic property of critical phenomena.
- Collective flow effects (directed, elliptic and higher ones) for hadrons including strange ones.
- Femtoscopic correlations of identical and non-identical species providing spatio-temporal characteristics of the freeze-out zone.
- Di-leptons yield as electromagnetic probes of a nuclear matter at high temperature/density.
- Positive/negative pion asymmetry with respect to the reaction plane as a probe such a fundamental problem as spontaneous violation of CP parity in strong interactions.

Primarily, an analysis of the measured yields and kinematical characteristics of particles produced in both peripheral and central collisions will be performed. These particles include charged hadrons ($\pi^+, \pi^-, K^+, K^-, p, \overline{p}$) measured directly and various neutral and charged strange particles (${K_s}^0, \Lambda, \Xi^-, \Omega^-$) identified via charged particle decay modes. A study of the corresponding particle yields and spectra as a function of the impact parameter (size of the reaction volume) will provide additional information about the signature for the formation of the dense nuclear matter. A study of the multiplicity fluctuations, femtoscopic correlations, and collective flows of identified hadrons allows one to extract information on **the nuclear equation of state** for baryonic matter at high density. The important observable for a signature of **chiral symmetry restoration** is the modification of the properties of vector mesons at high baryon density. Their in-medium properties can be studied by measuring the dileptonic decay channels.

In order to obtain a complete picture of heavy-ion collisions, the reference data from elementary collisions are required, so a comprehensive set of observables should be measured in

proton-nucleus and nucleus-nucleus collisions over the full NICA energy range. To get quantitative estimates of the expected particle yields and spectral shapes, the samples of events for the central and minimum bias Au+Au collisions at energies $\sqrt{s}_{NN} = 4, 5, 7, 9, 11\ GeV$ were simulated with the UrQMD [8] and FASTMC [5] codes.

3.1 Particles yield

Meson and hyperon multiplicity versus the collision energy in comparison with the AGS and SPS data are given in Fig. 3. Experimental data are represented by excitation function of particle multiplicities in Au+Au collisions at energy range E_{Lab} = 2 - 15 AGeV at AGS and in Pb+Pb collisions at E_{Lab} = 20 - 160 AGeV at SPS. As seen in Fig. 3, theoretical calculations depicted by open symbols overestimate the measured pion multiplicities and underestimate the kaon multiplicities (filled symbols). The yield of multistrange hyperons is underestimated by the UrQMD code as well.

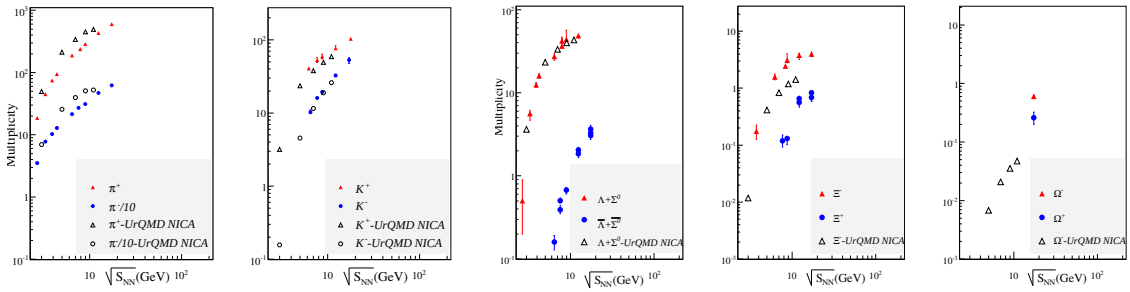

Figure 3: Meson and hyperon multiplicities in central ($b < 3$ fm) Au+Au (Pb+Pb) collisions at the energy range from AGS ($\sqrt{s} = 2.4 - 5.5 GeV$) [21] to SPS ($\sqrt{s} = 6.3 - 17.8 GeV$) [4] energies. The UrQMD calculation is plotted by open circles and triangles; the data - by corresponding filled symbols.

In the NICA energy range, one of the most promising observables that could serve as a sensitive diagnostic probe of two phases of matter created in the high energy heavy ion collisions is the strangeness-to-entropy ratio which can be estimated through the kaon-to-pion and/or Lambda-to-pion ratios. A pronounced peak of the K^+/π^+ ratio, the so-called "horn" effect, was discovered by the CERN-NA49 collaboration in central $Pb+Pb$ collisions at a beam energy of 30 AGeV (Fig. 4). The $(\Lambda + \Sigma^0)/\pi$ ratio exhibits a similar maximum at the same beam energy. Transport models, HSD (Hadron String Dynamics) and UrQMD, fail to describe these experimental data possibly due to insufficient number of resonances accounted for in the models [6]. Among the numerous particle species to be measured with the MPD, strange particles are of particular interest, since strangeness production has already proven to be a valuable diagnostic tool for investigating the QGP phase. It has been argued [15] that the onset of deconfinement in central heavy-ion collisions may manifest itself in a non-monotonic energy dependence of the strangeness-to-entropy ratio. As the K^+ yield is proportional to the overall strangeness production and the total entropy produced in the reaction can be associated with the pions, the K^+/π^+ ratio was proposed as the key observable. The experimental data, indeed, show an anomaly in the energy dependence of the strangeness to entropy ratio. The rapid increase of the relative kaon-to-pion multiplicity changes dramatically at $\sqrt{s_{NN}} \approx 8$ GeV, – the ratio drops down sharply (by about 30%) and then reaches some kind of saturation.

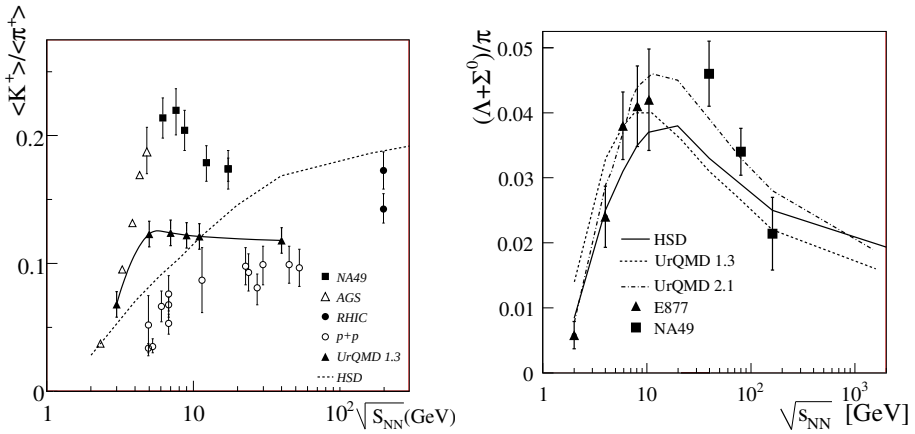

Figure 4: Left)K^+/π^+ ratio for central Au+Au (Pb+Pb) collisions. Right)Hyperon to pion ratio. The experimental data are from AGS, SPS and RHIC.

3.2 Particle Spectra

Despite the relatively good agreement of data and transport calculations in the longitudinal direction, significant deviations are found in the transverse direction. In addition to the enhanced relative yield of positive kaons, the measured transverse mass spectra of both positive and negative kaons around the center-of-mass rapidity at AGS and SPS energies show a substantial hardening in central Au + Au collisions relative to pp interactions. The m_t-distributions of kaons in nucleus-nucleus interactions can be treated as thermal; the inverse slope parameter, T, from an exponential in m_t fit is a measure of the effective temperature of the source:

$$\frac{1}{m_t}\frac{dN}{dm_t} = C\exp(-\frac{m_t - m}{T}) \tag{1}$$

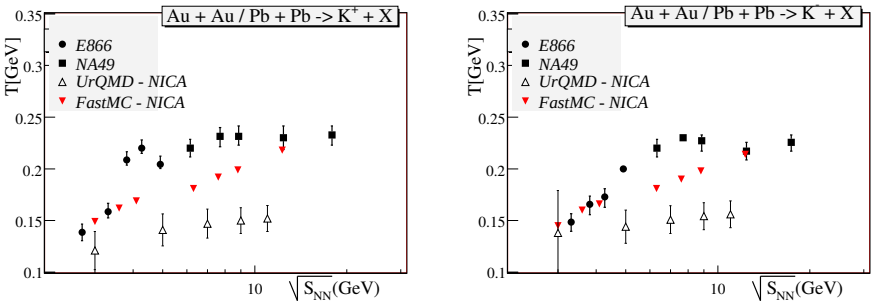

Figure 5: Inverse slopes of transverse momentum distributions for K^+ and K^- in central Au + Au and Pb + Pb collisions. UrQMD points are given for Au + Au collisions.

Fig. 5 displays the inverse slopes of transverse spectra of kaons in Au + Au and Pb + Pb collisions measured at AGS and SPS compared with UrQMD and FASTMC calculations, which considerably deviate from the data. The NICA/MPD detector combining the large

phase space coverage and excellent PID capabilities offers the exciting possibility to study in great detail transverse mass (m_t) and rapidity (y) dependence of hadron production. Detailed measurements of the excitation function of the effective temperature of the kaon spectra in different colliding systems (from p+p to central A+A) may help to identify a possible phase transition. In addition, an analysis of the m_t-spectra of several particle species (π, K, p) within hydrodynamics-motivated blast-wave approaches will provide valuable information on collective expansion of the colliding system.

3.3 Femtoscopy Correlations

The momentum correlations of two or more particles at small relative momenta in their center-of-mass (c.m.) system are widely used to study space-time characteristics of the production processes on a level of 10^{-15} m, so serving as a correlation femtoscopy tool [23, 24]. Usually, it is assumed that the correlation of two particles emitted with a small relative velocity is only influenced by the effects of their mutual quantum statistics and final state interaction. The primary goal of femtoscopy, performed at mid-rapidity and low transverse momentum, is to study the space-time size of the emitting source and freeze-out processes of the dynamically evolving collision system.

Experimentally, the two-particle correlation function reads

$$C(\vec{q}, \vec{K}) = \frac{A(\vec{q}, \vec{K})}{B(\vec{q}, \vec{K})}, \tag{2}$$

where $A(\vec{q}, \vec{K})$ is the distribution of pairs of particles with relative momentum $\vec{q} = \vec{p_1} - \vec{p_2}$ and average momentum $\vec{K} = (\vec{p_1} + \vec{p_2})/2$ from the same event, and $B(\vec{q}, \vec{K})$ is the corresponding distribution for pairs of particles taken from different events. The correlation function is normalized to unity at large $\vec{q}$. According to the "out-side-long" convention it is possible to measure three-dimensional decompositions of $\vec{q}$ [16, 25, 22, 7, 27, 11], providing better insight into the collision geometry. The relative momentum $\vec{q}$ is decomposed into the variables q_{long} along the beam direction, q_{out} parallel to the transverse momentum of the pair $\vec{k_t} = (\vec{p_{1t}} + \vec{p_{2t}})/2$, and q_{side} perpendicular to q_{long} and q_{out}. In the longitudinal co-moving system (LCMS) the correlation function in Eq. 2 can be decomposed as follows:

$$C(q_{out}, q_{side}, q_{long}) = 1 + \lambda \exp(-R^2_{out} q^2_{out} - R^2_{side} q^2_{side} - R^2_{long} q^2_{long}), \tag{3}$$

where LCMS Gaussian radii $R_{out}, R_{side}, R_{long}$. Assuming perfect experimental particle identification and a purely chaotic (incoherent) source, λ represents the fraction of correlated pairs. The correlation function can by expressed as a square of the properly symmetrized wave function (describing two-particle scattering) averaged over the relative separation in the pair rest frame

$$C(\vec{q}, \vec{K}) = \int d^3 r S_K(\vec{r}) |\phi(\vec{q}, \vec{r})|^2, \tag{4}$$

where $S_{K(r)}$ is the source function. Rather than fully inverting the measured correlation function to determine the $S_K(\vec{r})$, most analyzes fit to Gaussian forms for the source function,

$$S_K(\vec{r}) \sim \exp\{-\frac{x^2}{4R^2_{out}} - \frac{y^2}{4R^2_{side}} - \frac{z^2}{4R^2_{long}}\}, \tag{5}$$

and determine the three radius parameters $R_{out}, R_{side}, R_{long}$, which are all functions of $\vec{K}$. The ratio R_{out}/R_{side} is used to gauge the suddenness of the emission. More explosive collisions lead to both smaller R_{out}/R_{side} and smaller values of R_{long}.

It was demonstrated [32] that the particle spectra, interferometry volumes (correlation radii), and averaged phase-space densities, measured at any time of the expansion of hadron-resonance

gas, are approximately conserved upon isentropic and chemically frozen evolution. Studying femtoscopic correlations thus allows one to constrain the model predictions for early stages and fireball evolution. It was expected that the first order phase transition strongly delays the fireball evolution [28]. However, the pion correlation radii measured in a wide energy range from AGS to RHIC energies demonstrated surprisingly weak energy dependence and did not demonstrate any discontinuities. More detailed aspects of femtoscopic measurements are needed to clarify the space-time structure of the emitting sources: radii with respect to the reaction plane, correlations of other species, especially non-identical particles, and non-Gaussian features of the source function.

3.4 Electromagnetic Probes

The important observable for chiral symmetry restoration is the modification of the properties of vector mesons at high baryon density. Their in-medium properties can be studied by measuring the dileptonic decay channels. Dileptons represent a penetrating probe of the hot and dense nuclear matter created in heavy ion collisions. Since dileptons interact only electromagnetically,

i	Dilepton channel	
1	Dalitz decay of π^0:	$\pi^0 \to \gamma e^+e^-$
2	Dalitz decay of η:	$\eta \to \gamma e^+e^-$ (or $\mu^+\mu^-$)
3	Dalitz decay of ω:	$\omega \to \pi^0 e^+e^-$
4	Dalitz decay of Δ:	$\Delta \to Ne^+e^-$
5	direct decay of ω:	$\omega \to e^+e^-$
6	direct decay of ρ:	$\rho \to e^+e^-$
7	direct decay of ϕ:	$\phi \to e^+e^-$
8	direct decay of J/Ψ:	$J/\Psi \to e^+e^-$
9	direct decay of Ψ':	$\Psi' \to e^+e^-$
10	Dalitz decay of η':	$\eta' \to \gamma e^+e^-$
11	pn bremsstrahlung:	$pn \to pne^+e^-$
12	$\pi^\pm N$ bremsstrahlung:	$\pi^\pm N \to \pi N e^+e^-$, where $N = p$ or n

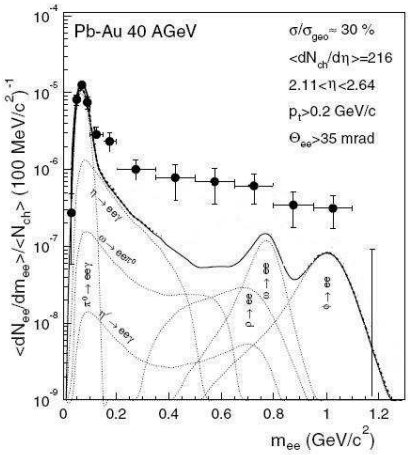

Figure 6: Left) Direct and Dalitz decay channels yielding dilepton pairs in central AuAu/PbPb collisions. Right)Data from CERES [2] with "hadronic cocktail" of dilepton sources.

their mean free path is large compared to the size of the system formed in these collisions. They are thus not distorted by final state interactions and once produced can escape unaffected the interaction region, carrying to the detectors information about the conditions and properties of the medium at the time of their creation. Analyzing invariant mass dilepton spectra, one can extract information on the modifications induced by the medium on specific properties of the vector meson, such as its mass and/or its width. Low-mass dileptons in nuclear collisions were measured in three different energy ranges: 1-2 AGeV at the DLS (BEVALAC) [26] and HADES (GSI) [30], 40 and 158 AGeV at the CERN SPS [2] as well as $\sqrt{s}_{NN} = 200$ GeV at RHIC [3]. All experiments observed an enhanced production of dileptons over a very broad invariant mass range of m_{ll} from $200\ MeV/c^2$ up to $700\ MeV/c^2$ (see right panel on Fig. 6). There are no measurements performed in the energy range E_{Lab} = 2-40 AGeV. It is very important to cover this energy gap, since an enhancement of low-mass dileptons are observed both at low (BEVALAC and HADES) and high (SPS) energies studied, and it is not clear that the enhancement reflects the same physics in all cases. The measurement of dileptons is notoriously difficult. There are two main difficulties. The first one is the huge combinatorial background of uncorrelated lepton pairs. It arises from the fact that, since single leptons do not preserve any information about their parent particle, all leptons are paired with all anti-leptons

in the same event to form the invariant mass spectrum. This background therefore depends quadratically on the particle multiplicity and strongly increases as the coverage moves to low-p_T leptons. In the measurement of e^+e^- pairs, the combinatorial background mainly comes from π^0 Dalitz decays and conversions. The second difficulty is the physics background. Photons and dileptons can be emitted by a variety of sources (left panel on Fig. 6), and therefore before claiming observation of any new effect, it is mandatory to have a thorough understanding of the expected contribution from all known sources. A lot of gammas is created due to electromagnetic decays of hadrons after the freeze-out. These gammas or leptons carry no information about excited system and usually should be subtracted ("hadronic cocktail"). One of the main tasks of NICA/MPD program is reconstruction of low mass vector mesons ρ, ω, ϕ by the measurements of their dileptonic decay channels.

3.5 Chiral Magnetic Effect

The system created in a noncentral relativistic nucleus-nucleus collision possesses large angular orbital momentum. Along with large angular orbital momenta the noncentral collisions may create magnetic fields due to relative motion of electrically charged ions and the products of the collision. The magnetic fields lead to other unusual effects due to nontrivial topological structure of QCD [17, 13, 18]. One of the most interesting effects, called the Chiral Magnetic Effect (CME), generates a spatial separation of positive and negative electric charges along the direction of the magnetic field. This effect being manifestation of P- and CP-violation in heavy ion collisions and predicted in the paper [19] has been indeed observed by the STAR Collaboration at RHIC in Au+Au and Cu+Cu collisions at = 200 GeV and 62 GeV [37, 1].The experimental results agree qualitatively with the theoretical predictions for local P-odd violation in heavy-ion collisions. Recently, these measurements were extended below the nominal RHIC energy down to $\sqrt{s_{NN}} = 7.7$ GeV within the RHIC Beam-Energy-Scan (BES) program [14].

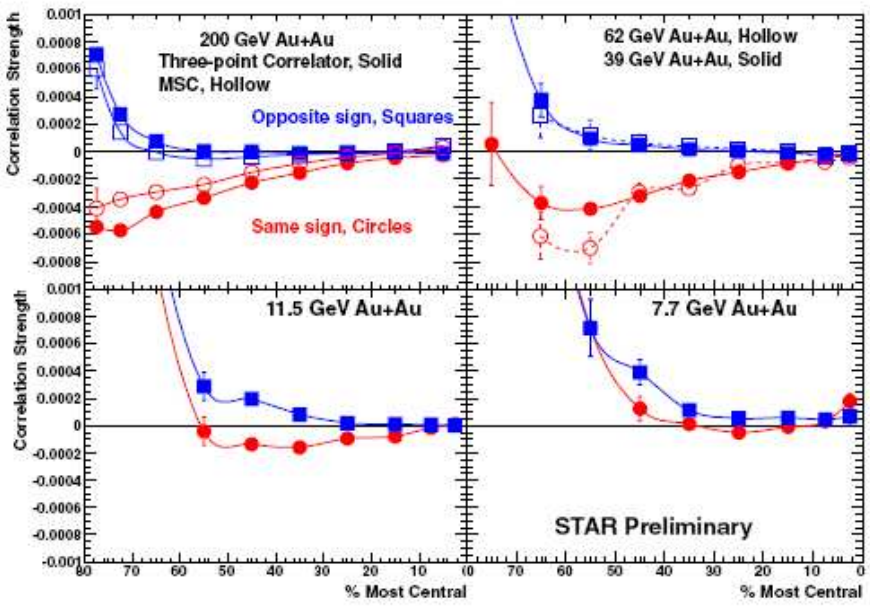

Figure 7: Energy dependence of the three-point correlator versus centrality for $\sqrt{s_{NN}} = 200$, 62, 11.5 and 7.7 GeV.

In the experiment the signal of the local parity violation is characterized by two body three-point correlator in the azimuthal angles,

$$a_{ij} = \langle cos(\varphi_i + \varphi_j - 2\Psi_{RP})\rangle = \langle cos(\varphi_i - \Psi_{RP}) cos(\varphi_j - \Psi_{RP})\rangle \langle sin(\varphi_i - \Psi_{RP}) sin(\varphi_j - \Psi_{RP})\rangle, \quad (6)$$

where $\varphi_{i,j}$ is the azimuthal angle of particles/antiparticles (for example, π^+ and π^-), Ψ_{RP} is the collision reaction plane angle and subscripts of a_{ij} represent the signs of electric charges being positive or negative. The CME implies an imbalance between total electric charge observed above and below the reaction plane which is indeed seen in data at $\sqrt{s_{NN}} = 200$ GeV. Fig. 7 shows the three-point correlator for four energies going down to $\sqrt{s_{NN}} = 7.7$ GeV. As the energy decreases we observe a decrease in the difference between opposite-charge and same-charge correlations. The authors explained the observed suppression of the opposite-charge correlations by the presence in the measurements of P-even background. In the description of the CME, two quantities have particular importance as the beam energy is decreased: the time integrated magnetic flux and the energy cut-off of chiral symmetry restoration. The observed signal can not be described by the background models used in [37, 1], however, alternative mechanisms resulting in a similar charge separation effect are not fully excluded (see e.g. Refs. [38, 31, 10]). A careful analysis of such a contribution is obviously needed before any strong conclusion can be drawn from these measurements. A detailed analysis of CME in the framework of transport models HSD and PHSD did not clarify this issue [36, 35].

There is an interesting counterpart of this effect, Chiral Vortaic Effect (CVE) [20] due to coupling to P-odd medium vorticity. Autors of the paper [29] suggest a straightforward generalization of CVE resulting in generation of all conserved-charge currents. They address the case of the baryonic charge and the corresponding asymmetries of baryons, especially neutrons (not affected by CME), which can be measured at NICA/MPD. Owing to the large baryonic chemical potential, appearing in the collisions at comparatively low energies at the FAIR and NICA (and possibly SPS and RHIC at low energy scan mode) facilities, the separation of the baryonic charge could be more preferable at these energies.

4 Conclusions

We presented scientific goals of the new JINR project NICA/MPD including a study in-medium properties of hadrons and the nuclear matter equation of state, a search for possible signatures of deconfinement and/or chiral symmetry restoration, phase transitions and QCD critical endpoint in the region of $\sqrt{s_{NN}} = 4$ - 11 GeV by means of careful scanning in beam energy, atomic number and centrality of the excitation functions. The measurements will include multiplicities and global characteristics of identified hadrons, such as: fluctuations in multiplicity and transverse momenta; directed and elliptic flows for various hadrons; femtoscopic momentum correlations; electromagnetic probes (photons and dileptons); asymmetry of particle electric charges (CME).

References

[1] B.I. Ableev et al. *Phys. Rev.*, C81:054908, 2010.

[2] D. Adamova et al. *Phys. Rev. Lett.*, 91:042301–1, 2003.

[3] D. Adare et al. *Phys. Rev. C*, 81:034911, 2010.

[4] C. Alt et al. Pion and kaon production in central Pb+Pb collisions at 20A and 30A GeV: Evidence for the onset of deconfinement. *Phys. Rev.*, C77:024903, 2008.

[5] N. S. Amelin et al. A Fast Hadron Freeze-out Generator. *Phys. Rev.*, C74:064901, 2006.

[6] D. Andronic, P. Braun-Munzinger, and J. Stachel.

[7] G. F. Bertsch, P. Danielewicz, and M. Herrmann. *Phys. Rev.*, C49:442, 1994.

[8] M. Bleicher et al. Relativistic hadron hadron collisions in the ultra- relativistic quantum molecular dynamics model. *J. Phys.*, G25:1859–1896, 1999.

[9] N Bogolubov, B. Struminsky, and A. Tavkhelidze. *JINR D-1968, Dubna*, 1965.

[10] A. Bzdak, V. Koch, and J. Liao. *Phys. Rev.*, C 81:031901, 2010.

[11] S. Chapman, P. Scotto, and U. Heinz. *Phys. Rev. Lett.*, 74:4400, 1995.

[12] Z. Fodor and S. D. Katz. Critical point of QCD at finite T and mu, lattice results for physical quark masses. *JHEP*, 04:050, 2004.

[13] K. Fukushima, D. E. Kharzeev, and H. J. Warringa. *Phys. Rev.*, D 78:074033, 2008.

[14] Dhevan Gangadharan. *J. Phys. G: Nucl. Part. Phys.*, 38:124166, 2011.

[15] M Gazdzicki and M. Gorenstein. *Acta Phys. Polon.*, B30:2705, 1999.

[16] P. Grassberger. *Nucl. Phys.*, B120:231, 1977.

[17] D. E. Kharzeev, L. D. McLerran, and H. J. Warringa. *Nucl. Phys.*, A 803:227, 2008.

[18] D.E. Kharzeev. *Phys. Lett.*, B 633:260, 2006.

[19] D.E. Kharzeev, R.D. Pisarski, and M.H.G. Tytgat. *Phys. Rev. Lett.*, 81:512, 1998.

[20] D.E. Kharzeev and A. Zhitnitsky. *Nucl. Phys.*, A 797:67, 2007.

[21] J. L. Klay et al. *J. Phys. ReV.*, C 68:054905, 2003.

[22] P. Lednicky. *JINR Comm., B2-3-11460.*

[23] R. Lednicky. *Phys. of Atomic Nuclei*, 67:71, 2004.

[24] R. Lednicky. Femtoscopic correlations in multiparticle production and beta-decay. *Braz. J. Phys.*, 37:939–948, 2007.

[25] M. I. Podgoretsky. *Sov. J. Nucl. Phys.*, 37:272, 1983.

[26] R. J. Porter et al. *Phys. Rev. Lett.*, 79:1229, 1997.

[27] S. Pratt. Two particle and multiparticle measurements for the quark - gluon plasma. In Hwa, R.C. (ed.): Quark-gluon plasma, vol.2, 700-748.

[28] Dirk H. Rischke and Miklos Gyulassy. The time-delay signature of quark-gluon plasma formation in relativistic nuclear collisions. *Nucl. Phys.*, A608:479–512, 1996.

[29] O. Rogachevsky, A. Sorin, and O. Teryaev. *Phys. Rev.*, C 82:054910, 2010.

[30] A. Rustamov et al. *Int. Jour. Mod. Phys. A*, 26:384, 2011.

[31] S. Schlichting and S. Pratt.

[32] Yu. M. Sinyukov, S. V. Akkelin, and Yogiro Hama. On freeze-out problem in hydro-kinetic approach to A+A collisions. *Phys. Rev. Lett.*, 89:052301, 2002.

[33] M. A. Stephanov. QCD phase diagram: An overview. *PoS*, LAT2006:024, 2006.

[34] A. Tavkhelidze. *High Energy Physics and Elementary Particles, Vienna*, page 753, 1965.

[35] V. D. Toneev et al.

[36] V. D. Toneev et al. *Phys. Rev.*, C 85:034910, 2012.

[37] S.A. Voloshin. *Nucl. Phys.*, A830:377c, 2009.

[38] F. Wang. *Phys. Rev.*, C 81:064902, 2010.